Journal of Magnetic Resonance 354 (2023) 107539

Contents lists available at ScienceDirect

Journal of Magnetic Resonance

journal homepage: www.elsevier.com/locate/jmr

Studies of proline conformational dynamics in IDPs by ^{13}C-detected cross-correlated NMR relaxation

Marco Schiavina [a], Ruth Konrat [b], Irene Ceccolini [b], Borja Mateos [b], Robert Konrat [b,*], Isabella C. Felli [a,*], Roberta Pierattelli [a,*]

[a] Department of Chemistry "Ugo Schiff" and Magnetic Resonance Center, University of Florence, Via Luigi Sacconi 6, 50019 Sesto Fiorentino, Florence, Italy
[b] Department of Structural and Computational Biology, University of Vienna, Max F. Perutz Laboratories Vienna Biocenter Campus 5, 1030 Vienna, Austria

ARTICLE INFO

Keywords:
^{13}C direct detection
Proline
Cross correlation
Dynamics
Intrinsically disordered proteins

ABSTRACT

Intrinsically disordered proteins (IDPs) are significantly enriched in proline residues, which can populate specific local secondary structural elements called PPII helices, characterized by small packing densities. Proline is often thought to promote disorder, but it can participate in specific π·CH interactions with aromatic side chains resulting in reduced conformational flexibilities of the polypeptide. Differential local motional dynamics are relevant for the stabilization of preformed structural elements and can serve as nucleation sites for the establishment of long-range interactions. NMR experiments to probe the dynamics of proline ring systems would thus be highly desirable. Here we present a pulse scheme based on ^{13}C detection to quantify dipole–dipole cross-correlated relaxation (CCR) rates at methylene CH_2 groups in proline residues. Applying ^{13}C-CON detection strategy provides exquisite spectral resolution allowing applications also to high molecular weight IDPs even in conditions approaching the physiological ones. The pulse scheme is illustrated with an application to the 220 amino acids long protein Osteopontin, an extracellular cytokine involved in inflammation and cancer progression, and a construct in which three proline-aromatic sequence patches have been mutated.

1. Introduction

Intrinsically disordered proteins (IDPs) play crucial roles in protein interaction networks and are thus of central importance for eukaryotic life. Consequently, efforts are ongoing in the nuclear magnetic resonance (NMR) community and beyond to study their solution structural dynamics and interactions with binding partners [1–8]. Despite their substantial overall dynamics, IDPs are far from randomly disordered and structural preformation prevails as a result of the geometric properties of the protein backbone and of long-range interactions that can be driven for example by electrostatics. The major distinction between globular proteins and IDPs, which results directly from their notable primary sequence diversity, resides in the relative energies of well-defined local minima (conformations) and the energy barriers that separate them [9,10]. In contrast to globular proteins that contain significant fractions of hydrophobic amino acids, IDPs are rich in amino acids with either polar or charged amino side-chains, as well as in proline residues [11–15]. While there is ample evidence that proline residues are disorder promoters we have recently performed an NMR study on Osteopontin (OPN) [16] that calls for a reassessment of the structural and functional role of proline residues in IDPs. Despite the absence of local secondary structure elements, OPN can be considered as not entirely disordered. It has indeed been shown that this protein possesses a central compact region that seems to be promoted by specific interactions between proline and aromatic amino acid side chains [3,16]. This suggests that these motifs might serve as nucleation sites for the formation of compact states in IDPs [16]. To get insights on the structural dynamics and the functional roles of proline residues in IDPs, more sophisticated and information-rich NMR techniques are needed.

Given its unique cyclic structure (pyrrolidine ring) and the resulting lack of an amide proton, conventional NMR schemes based on $^{1}H^{N}$ detection are not so effective to characterize proline residues in proteins. Moreover, the sensitivity of methods relying on amide proton detection is significantly impaired when pH and temperature conditions approximate the physiological ones. Alternative approaches have been developed to investigate these proteins in their native conditions as well as upon interaction and partially overcome this limitation [17–24].

Due to the availability of ^{13}C/^{15}N-enriched recombinant proteins

* Corresponding authors.
E-mail addresses: robert.konrat@univie.ac.at (R. Konrat), felli@cerm.unifi.it (I.C. Felli), roberta.pierattelli@unifi.it (R. Pierattelli).

https://doi.org/10.1016/j.jmr.2023.107539
Received 4 July 2023; Received in revised form 7 August 2023; Accepted 9 August 2023
Available online 11 August 2023

and thanks to major technological advances in cryogenically cooled dedicated probes for the direct detection of heteronuclei [25] the use of ^{13}C detected NMR to study macromolecules has become a very attractive and used alternative [20, 26–29]. Particularly, 2D correlation of carbonyl carbon and amide nitrogen nuclear spins across the peptide bond (C'_i-N_{i+1}) results in exquisite signal dispersion [30,31]. This is largely independent of the presence of tertiary structure and provides information about all amino acids, including proline. Consequently, so-called CON-based spectra have been established as the most complete two-dimensional fingerprint of an IDP [20,32–34].

Here we make use of direct ^{13}C-detection tools and combine them with cross-correlated NMR spin relaxation experiments to probe proline ring dynamics in IDPs by quantifying $^{13}CH_2$-methylene dipole–dipole cross-correlated relaxation (CCR). Typically, CCR effects can be observed between two different dipolar (D) interactions (D-D), two different chemical shift anisotropies (CSA-CSA) or between a dipolar and a chemical shift anisotropy (D-CSA) interaction. Interference effects between fluctuations of different relaxation mechanisms of the same tensor rank (rank 2) have been shown to be a valuable source of information about the structure and dynamics of proteins since they are related to their relative geometries [35,36]. The pulse sequence for measuring $^{13}CH_2$-methylene dipole–dipole cross-correlated relaxation in prolines is illustrated with an application to OPN. Data were recorded for the construct comprising residues 45-264 of OPN (WT hereafter) and a triple-mutant (F121A/F130A/W184A) form in which important and structurally relevant π·CH interaction between aromatic side chains and proline rings are abrogated due to the mutation of aromatic residues into alanine ones (TM hereafter). The observed differential dynamics in these forms of OPN provide further evidence for the relevance of these sequence motifs and proline ring interactions for the formation of compacted substrates in IDPs. These interactions are mediated by the puckering of the pyrrolidine ring in proline residues and its characterization is of interest for describing this phenomenon.

2. Methods

2.1. Sample preparation

pET11d plasmid containing the *Coturnix japonica* (quail) OPN sequence was transformed into the *E.coli* strain BL21(DE3) phage resistant via heat-shock method. Protein expression was induced at OD600 of ca. 0.8 by adding 0.4 mM IPTG (Isopropyl-β-D-Thiogalactopyranoside). For expression of isotopically labelled protein for NMR studies, before induction the cells were harvested and pellets from 4L LB resuspended in 1L M9-Minimal Media (containing 1 g/L $^{15}NH_4Cl$ and 3 g/L ^{13}C-Glucose for ^{15}N and ^{13}C labelling respectively). The expression was carried out at 27 °C and 140 rpm over-night. The cells were harvested and resuspended in 40 mL of cold PBS (2 mM KH_2PO_4, 8 mM Na_2HPO_4, 2.5 mM KCl, 140 mM NaCl, 5 mM EDTA, pH 7.3). The suspension was sonicated and heated at 95 °C for 10 min. The lysate was centrifuged at 18000 rpm and an ammonium sulphate precipitation (saturation of 50%) carried out with the supernatant. The pellet was resuspended in PBS, diluted 1:2 with water to lower the salt concentration and an anion-exchange chromatography (HiTrap Q, GE healthcare) performed. The column was equilibrated with PBS and a gradient of 30% High-Salt Buffer (PBS containing 1 M NaCl) run in 20 min at 2 mL/min. Protein purity was confirmed via SDS-PAGE electrophoresis. The protein was concentrated using a centrifugal filter and the final concentration measured at 280 nm. The final WT OPN sample concentration was 2.2 mM. The TM OPN sample was 1.3 mM.

2.2. ^{13}C-detected cross correlation rates experiments

NMR experiments were recorded at 310 K with a Bruker AVANCE NEO instrument operating at 700.06 MHz ^{1}H, 176.03 MHz ^{13}C and 70.94 MHz ^{15}N frequencies exploiting a cryogenically cooled probehead optimized for ^{13}C-direct detection (TXO).

The ^{13}C carrier was placed at 176.7 ppm, 57.7 ppm, 45.1 ppm for C′, C^{α} and C^{δ} respectively, the ^{15}N carrier at 137 ppm and the ^{1}H carrier at 3.5 ppm (H^{α}) or 7.5 (H^{N}). For the CCR-CON^{Pro} experiment the following band-selective pulses were used: 300 μs with Q5 and time reversed Q5 shapes [37] for C′ and C^{δ} excitation, 220 μs Q3 shape [37] for C′/C^{δ} inversion/refocusing. A 900 μs Q3 shaped pulse was also used to be selective on C^{α} only. An adiabatic π pulse to invert both C′ and C^{ali} was used (smoothed chirp 500 μs, 20% smoothing, 80 kHz sweep width, 11.3 kHz radio frequency field strength). Homonuclear virtual decoupling in the direct dimension was achieved through the IPAP approach [38] acquiring the in-phase (IP) and antiphase (AP) components and properly combining them.

The experiment was acquired with a recycle delay of 1.6 s. 8 scans per increment and sweep widths of 30.0 ppm ^{13}C′, 7.4 ppm ^{15}N and 40.0 ppm $^{13}C^{ali}$ were used acquiring 1024 × 24 × 400 points in the three dimensions, respectively.

2.3. Proline ^{15}N R_2 experiments

The NMR experiments to determine the ^{15}N R_2 relaxation values for the proline residues were recorded at 700.06 MHz ^{1}H, 176.03 MHz ^{13}C and 70.94 MHz ^{15}N frequencies exploiting a cryogenically cooled probehead optimized for ^{13}C-direct detection (TXO). The ^{15}N R_2 experiments were performed using the previously reported ^{13}C detected pulse sequence [32], with 16 scans per increment and sweep widths of 30.0 ppm ^{13}C′ × 7.4 ppm ^{15}N acquiring 1024 × 128 real points in the two dimensions. A relaxation delay of 1.5 s has been used. To determine the ^{15}N R_2 values, the following delays were used both for WT OPN and for TM OPN samples: 160 ms, 240 ms, 320 ms, 400 ms, 480 ms, 560 ms, 640 ms, 800 ms. The R_2 values were determined fitting the data following equation: $I(t) = I(0)e^{-t/T_2}$, with $R_2 = \frac{1}{T_2}$.

2.4. Triple mutant assignment

NMR experiments to assign the triple mutant construct were recorded on a Bruker AVANCE III spectrometer operating at 950.20 MHz ^{1}H, 238.93 MHz ^{13}C, and 96.28 MHz ^{15}N frequencies, equipped with a cryogenically cooled probehead optimized for ^{1}H-direct detection (TCI). The 3D (H)CBCACON [39] was acquired with an interscan delay of 1.1 s. This spectrum was acquired with 2 scans, with sweep widths of 22.0 ppm ^{13}C′ x 36.0 ppm ^{15}N × 55.9 ppm $^{13}C^{ali}$ and 1024 × 192 × 96 real points in the three dimensions, respectively. The 3D (H)CBCANCO [39] was acquired with the very same acquisition parameters but for the number of scans. Four scans per increment were used for this experiment.

3. Results and discussion

3.1. The CCR-CON^{Pro} newly designed pulse sequence

From the NMR point of view, the detection of proline residues can be easily achieved through the CON experiment. Indeed, this experiment enables the obtainment of very clean and well-resolved spectra (Fig. 1A) and has the advantage to include signals from proline residues (Fig. 1B). The latter residues are central to this work and their position in the polypeptide and in the primary sequence of OPN is shown in Fig. 1C and 1D, respectively. Capitalizing on previously reported schemes for probing cross-correlated relaxation (CCR) in side chains of different proteins [40–42], we propose here a pulse sequence to quantify $^{13}CH_2$ dipole–dipole cross-correlation effects ($\Gamma_{CH1|CH2}$) in proline side chains (Fig. 2). This pulse scheme combines selection of proline residues through the (H)CCCdNCO experiment [43] with an additional element to quantify CH_2 CCRs [40], and we dubbed it CCR-CON^{Pro}.

Starting from aliphatic ^{1}H magnetization, a first magnetization

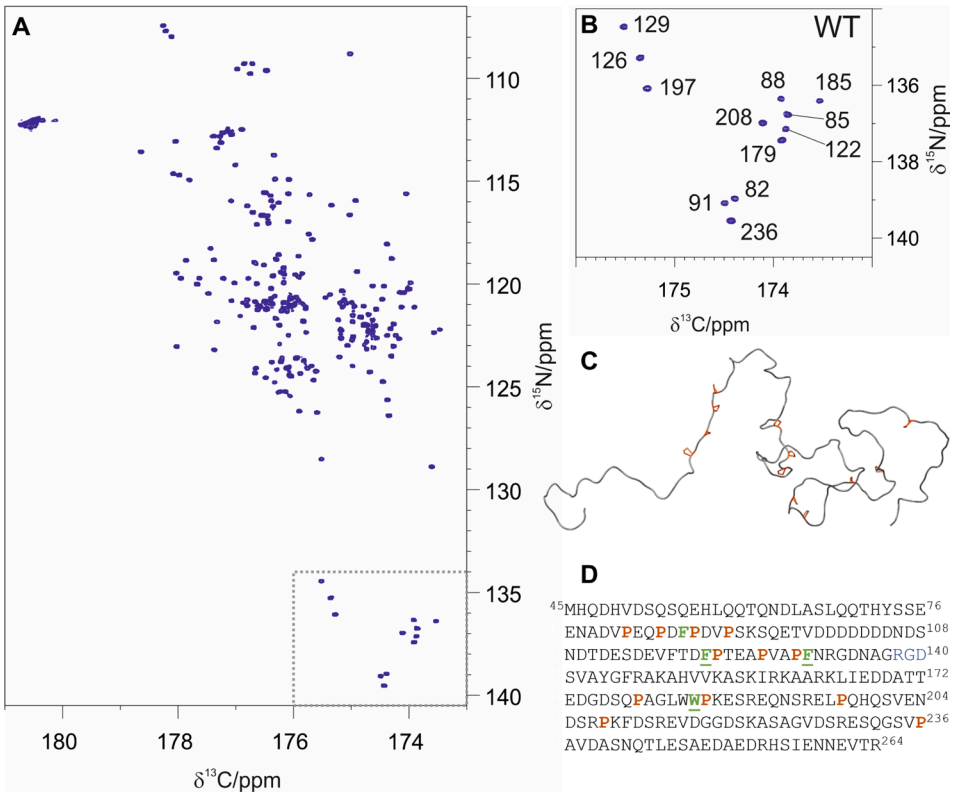

Fig. 1. A) ^{13}C-detected 2D CON spectrum recorded on WT OPN. The dotted grey square indicates the position of the resonances arising from the $^{13}C_{i-1}$-$^{15}N_i^{PRO}$ pairs; B) expansion of the proline region of the 2D CON spectrum reported in A with the corresponding assignment of the major form (numbered according to the P positions in the sequence); C) one of the possible conformations of the protein obtained with the statistical coil generator *Flexible Meccano* [44] highlighting the position of the proline residues; D) primary sequence of WT OPN. Proline residues are in red. Aromatic residues near a proline are in green and those three mutated in TM OPN are underlined.

Fig. 2. CCR-CON^{Pro} pulse sequence used to measure the cross correlation effect $\Gamma_{CH1|CH2}$ for the different CH spin systems in the proline ring (i.e. $\Gamma C_\beta H_{2\beta}|C_\beta H_{1\beta}$, $\Gamma C_\gamma H_{2\gamma}|C_\gamma H_{1\gamma}$, $\Gamma C_\delta H_{2\delta}|C_\delta H_{1\delta}$,). The delays used are $\Delta_2 = 3.6$ ms, $\Delta_3 = 0.95$ ms, $\Delta_4 = 7.1$ ms, $\Delta = 25.0$ ms, and $\Delta_1 = 9.0$ ms. The phase cycle is: φ_1 = y, -y, φ_2 = 4(y),4(-y), φ_3 = 2(x), 2(-x), φ_4 = 8(x), 8(-x), φ_{IP} = x; φ_{AP} = - y; φ_{rec} = x, -x, -x, x, -x, x, x, -x. Flopsy-16 spinlock block is used to transfer the magnetization across side chain of proline. Quadrature detection in F1 and F2 is obtained by incrementing φ_2 and φ_3 in a States-TPPI manner, respectively. The experiment was acquired at 310 K exploiting a 16.4 T instrument equipped with a cryogenically cooled probehead optimized for ^{13}C-direct detection (TXO). The C^{ali}, C^{δ} and C′ carriers were set 45.1 ppm, 57.7 ppm and 176.7 ppm respectively, the $^1H^{\delta}$ carrier at 3.5 ppm. The rounded black shapes and the squared shapes describe the shaped and hard pulses in the figure respectively. The thinner and thicker shapes represents π/2 and π pulses respectively. The following band-selective pulses were used: 300 μs with Q5 and time reversed Q5 shapes [37] for C′ and C^{δ} excitation, 220 μs Q3 shape [37] for C′/C^{δ} inversion/refocusing. A 900 μs Q3 shaped pulse (hashed shape in the figure) was also used to be selective on C^{α} only. An adiabatic π pulse with a smoothed chirp shape, 500 μs length, 20% smoothing, 80 kHz sweep width and 11.3 kHz radio frequency field strength was used to invert both C′ and C^{ali} (grey pulse in the figure). Homonuclear virtual decoupling approach in the direct dimension was achieved through the IPAP approach [38] acquiring the in-phase (IP - upper box in the figure) and antiphase (AP - lower box in the figure) components and properly combining them. The experiment was acquired with a recycle delay of 1.6 s. 8 scans per increment and sweep widths of 30.0 ppm ^{13}C′, 7.4 ppm ^{15}N and 40.0 ppm $^{13}C^{ali}$ were used acquiring 1024 × 24 × 400 points in the three dimensions respectively.

transfer is achieved via scalar coupling to the directly attached ^{13}C. This period is followed by an interval for ^{13}C antiphase refocusing. The desired magnetization is stored along the *z* axis and a purge gradient is applied to clean from unwanted contributions. Following the $\pi/2$ pulse, a C_x operator is created. From point *a* to *b* in the scheme depicted in Fig. 2, the evolution of the ^{13}C chemical shift is achieved in a constant time (CT) manner, set to n/J^{CC} (with *n* integer number) to avoid resolved carbon–carbon scalar couplings ($^1J^{CC}$) in the indirect dimension. In the very same period, the $^1J^{CH}$ is evolved. This allows us to resolve the ^{13}C multiplet components and to determine the cross correlation rate of the dipole–dipole interaction between the two CH bond vectors within the CH_2 group (CH^1 and CH^2), referred as $\Gamma_{CH1|CH2}$, as previously proposed [40]. At the end of this period, the desired magnetization is stored along the z axis and a second purge gradient is applied. Exploiting an isotropic mixing scheme (FLOPSY-16 [45]), the magnetization is transferred along the side chain and in particular to the C^δ nucleus. At this point, the magnetization follows the (H)CCCdNCO [43] pathway exploiting the uniqueness of proline residues' pyrrolidine ring, with the magnetization transferred from C^δ to N making use of the $^1J^{C\delta N}$ scalar coupling. Nitrogen chemical shift is thus encoded in the second indirect dimension. Finally, individual peptide bond signals ($C'_{i-1}N_i$) are observed following the classical CON detection scheme including the IPAP [38] building-block for $J^{C'C\alpha}$ decoupling.

Fig. 3A shows a schematic representation of the 3D spectrum obtained with the CCR-CON^{Pro} sequence, together with a representative plane (Fig. 3B) and the resulting trace for proline 208 (Fig. 3C) acquired on WT OPN.

Proline residues in OPN are not evenly distributed in the primary sequence (Fig. 1D). In the first half of the sequence, there are two clusters comprising a total of 7 proline residues; in the second half these are more spread, but two of them are close in sequence. The presence of pairs involving aromatic and proline residues has been proposed to be one of the driving forces that allow the formation of a compact state in OPN which involves three different regions encompassing residues 105–130, 140–160 and 175–190 [16]. We designed a triple mutant (TM) in which the aromatic residues of pairs $^{121}FP^{122}$, $^{184}WP^{185}$ and $^{129}PF^{130}$ are mutated into alanine residues.

The CON spectrum of the resulting TM OPN is similar to the WT one; nevertheless, there are local but significant variations which required the reassignment of the spectrum, obtained by recording the complementary 3D-(H)CBCACON and 3D-(H)CBCANCO experiments [39]. The assignment is reported in the supplementary material (Table S1), while in Fig. 4A the assignment of the signals in the proline regions is reported. With the same experiments and comparing the previously available assignment of the WT with the TM one, we were able to assign the minor forms arising from the presence of the *cis* isomer of the proline residues as well (Fig. 4B).

3.2. Proline ^{15}N R_2 and CCR results

^{15}N relaxation has been extensively used to achieve dynamic information in IDPs [46–50]. However no information about proline residues can be achieved through the widely used approach based on $^1H^N$ detection. Determination of the transverse relaxation rates of proline ^{15}N was performed to evaluate the differential local dynamics within WT OPN and to estimate how these changes in TM OPN. The ^{15}N R_2 relaxation rates obtained for the two proteins are reported in Fig. 5. As it can be noted, the major variations are found for P122, P208, and P236, which experience a reduction in the relaxation rates in the TM with respect to the WT, and for P88 and P197 which instead show increased R_2 values.

Next, the CCR values obtained with the new pulse sequence were analyzed. The traces for the different proline residues were extracted (Fig. S1) and the intensities of the three resolved multiplet components of the CH_2 signals measured. The CCR values were obtained following the approach proposed by Yang and co-workers [40]:

$$\Gamma_{CH_1|CH_2} = -\frac{1}{4T}\ln\left\{\frac{4I_{\alpha\alpha}(T)I_{\beta\beta}(T)}{\left[I_{\alpha\beta+\beta\alpha}(T)\right]^2}\right\}$$

where T is the duration of the constant time period (equal to n/J^{CC}, 28.4 ms with $n = 1$), $I_{\alpha\alpha}(T)$, $I_{\beta\beta}(T)$ and $I_{\alpha\beta+\beta\alpha}(T)$ the intensities of the two external and the central components of the triplet respectively. It's worth noting that the contribution of additional cross correlated relaxation rates (such as the $\Gamma_{C|CH_1} + \Gamma_{C|CH_2}$) to the multiplet components, responsible for asymmetries, will not contribute to the analysis. In cases of resonance overlap the data were not analyzed.

The obtained values are reported in Tables S2 and S3

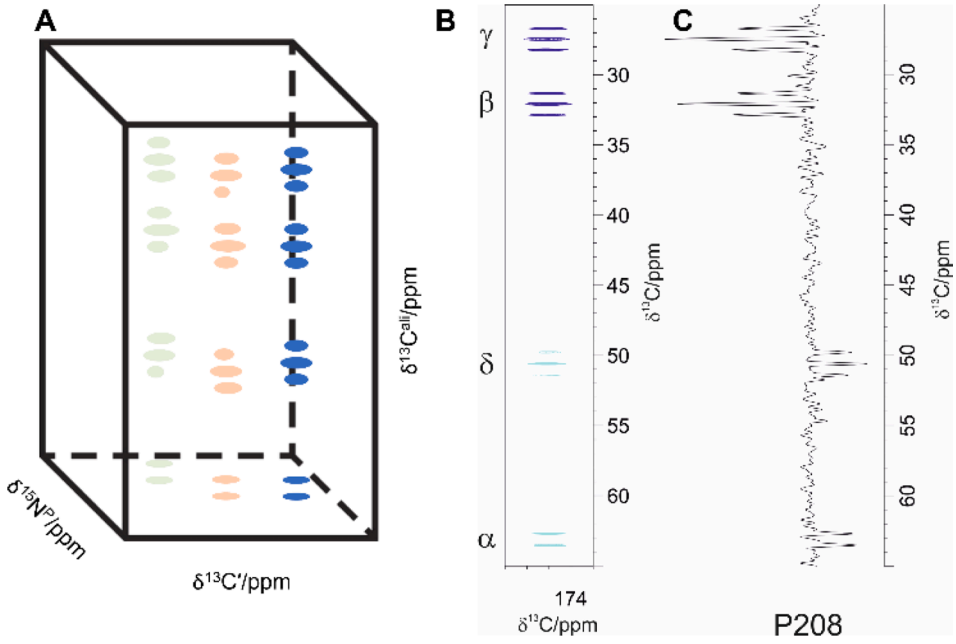

Fig. 3. A) Schematic representation of a CCR-CON^{Pro} spectrum; B) plane of the 3D spectrum showing the different triplet components as obtained with the proposed pulse sequence; C) resulting projection of the traces of the signals present in panel B arising from proline 208.

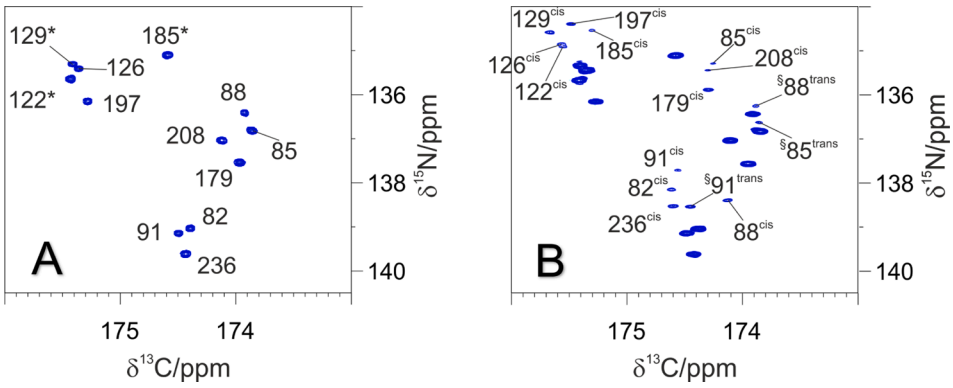

Fig. 4. A) Proline region in the 2D CON spectrum recorded on TM OPN. The main forms of prolines are observed and their assignment reported; B) lowering the contours also the signals of the minor forms appear. The mutated residues are marked with an asterisk. A second minor form for P85, P88 and P91 is detected as well and marked with §.

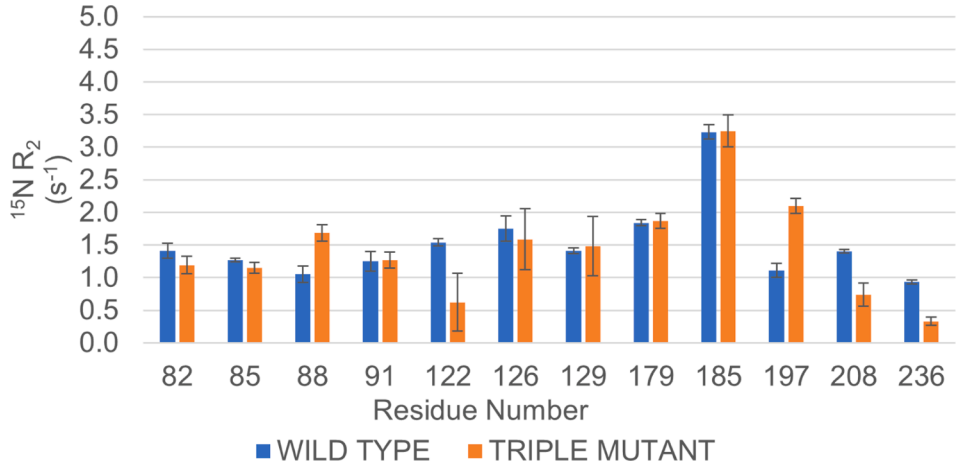

Fig. 5. A) ^{15}N R_2 values obtained for the WT (blue) and TM (orange) OPN constructs. B) Difference in ^{15}N R_2 between WT and TM.

(Supplementary material) for WT and TM OPN, respectively. All the obtained CCRs for the $C^{\beta}H_2$ spin systems display negative values while the CCRs for the $C^{\gamma}H_2$ spin systems present both positive and negative values. The CCR values obtained for the $C^{\gamma}H_2$ and the $C^{\beta}H_2$ are reported in Fig. 6. Moving to the triple mutant and comparing the signals obtained with the proposed pulse scheme, few changes are observed. The values are compared to the WT ones in Fig. 6. In particular P122, P129, P197, and P236 present slightly different behavior in the triplet shape of the $C^{\beta}H_2$ system with the latter proline residue displaying a more defined 1:2:1 shape for the triple mutant. P197 displays a different behavior for the $C^{\gamma}H_2$ system as well resulting more symmetrical in the triple mutant with respect to the wild type. P197 is found to be perturbed in both the $C^{\beta}H_2$ and $C^{\gamma}H_2$ pattern (Fig. S1). Although, there is an overall correlation between changes in motional dynamics probed by conventional ^{15}N spin relaxation (^{15}N R_2) and $^{13}CH_2$ CCR rates, experimental CCRs seem to be additionally sensitive to subtle changes of proline ring pucker dynamics not revealed by classical ^{15}N R_2 relaxation experiments given the differential fluctuation motions sensed by these two relaxation proxies.

3.3. Dynamic interpretation of CCR values

Experimental CCR values were interpreted and quantitatively analyzed using the theoretical formalism developed for proline by Mayo and co-workers [51]. This was proposed for globular proteins and, under the assumption that the overall correlation time refers to local motion of the peptide segment, it can also be extended to IDPs. Data from various IDPs of different length suggest that NMR relaxation is dominated by local, segmental motions [52–54]. Internal motion refers to ring dynamics. In the treatment proposed by Mayo and co-workers [51] a generalized order approach following the pioneering work of Lipari and Szabo is used [55] where the order parameter of the internal (local) dynamic is related to proline ring pucker motions. Capitalizing on previous work by London [56] and Shekar and Easwaran [57] ring pucker dynamics can be described by a two-state (A and B, *endo*-exo interconversion) jump model with corresponding lifetimes τ_A and τ_B, and a general jump angle Δ. The exact expressions for the cross-correlation order parameter S^2_{ab} and the corresponding C^{β}, C^{γ} and C^{δ} $^{13}CH_2$ dipole–dipole cross-correlation rate Γ_{CH1CH2} were taken from the original paper [58]. As was described earlier [59] while C^{β} is always negative the C^{γ} cross-correlation rate changes its sign depending on the motional parameter and is therefore most informative. The experimental CCR values were numerically analyzed by finding the optimal combinations of the relevant motional parameters: overall correlation time τ_0, internal correlation time τ_i, lifetimes τ_A and τ_B and general jump angle Δ. While τ_0, internal correlation time τ_i, lifetimes τ_A and τ_B were the same for a given proline residue, the general jump angle was individually optimized for the various carbon atoms C^{β}, C^{γ} and C^{δ} of the proline ring ($\Delta\beta$, $\Delta\gamma$ and $\Delta\delta$). To this end, a multi-dimensional grid search was performed varying all parameters independently. The optimal solution was assessed via a χ^2 (mean squared deviation between calculated and experimental CCR values). The following constraints in the grid search were employed based on previous findings [58]: the upper limits for the correlation times of the slowest (τ_0) and fast internal (τ_i) dynamical

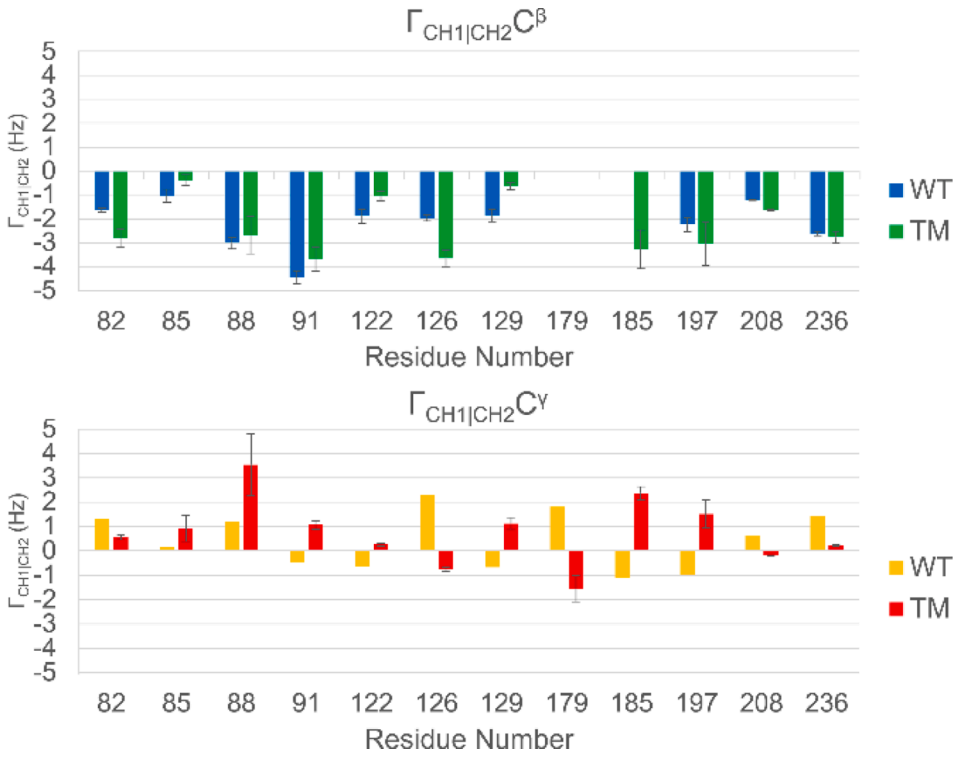

Fig. 6. Graphs reporting the $\Gamma_{CH1|CH2}$ values for different spin systems. The panels report the $\Gamma_{CH1|CH2}$ for $C^{\beta}H_2$ and $C^{\gamma}H_2$ spin system in blue and yellow for WT OPN and in green and red for TM OPN.

modes were set to 3000 ps and 100 ps, respectively; the internal jump angles fulfill the condition ($\Delta\beta < \Delta\gamma$). Due to limited signal-to-noise C^{δ} rates were omitted from the analysis.

It should be noted that we do not attempt to provide a comprehensive analysis of the motional dynamics of the different proline residues in OPN, but rather we want to relate the observed differential changes in CCRs to modification of the most relevant motional parameters (i.e. changes in correlation time τ_i of the fast intramolecular dynamical mode vs modulation of ring pucker, τ_A and τ_B). The obtained results are summarized in Table S4 (Supplementary Material) and shown in Fig. 7.

Comparison of the obtained motional parameters between wild-type and triple-mutant revealed no significant changes in τ_0 (in agreement with nearly unchanged ^{15}N transverse relaxation rates, Fig. 5) and jump angles $\Delta\beta$ and $\Delta\gamma$ (Fig. S2). Average values for $\Delta\beta$ and $\Delta\gamma$ were between 25° and 40° and in agreement with previous findings [58]. The most significant changes (larger than 0.2) in τ_A/τ_B ratios (ring puckering) were observed for residues 82, 122, 126 and 236, accompanied by smaller internal (τ_i) correlation times for the triple-mutant (particularly residues 82, 91, 122 and 185). The dynamical analysis thus revealed an interesting difference in ring puckering dynamics upon mutation, originating from the different interconversion equilibrium between the *endo*-exo forms.

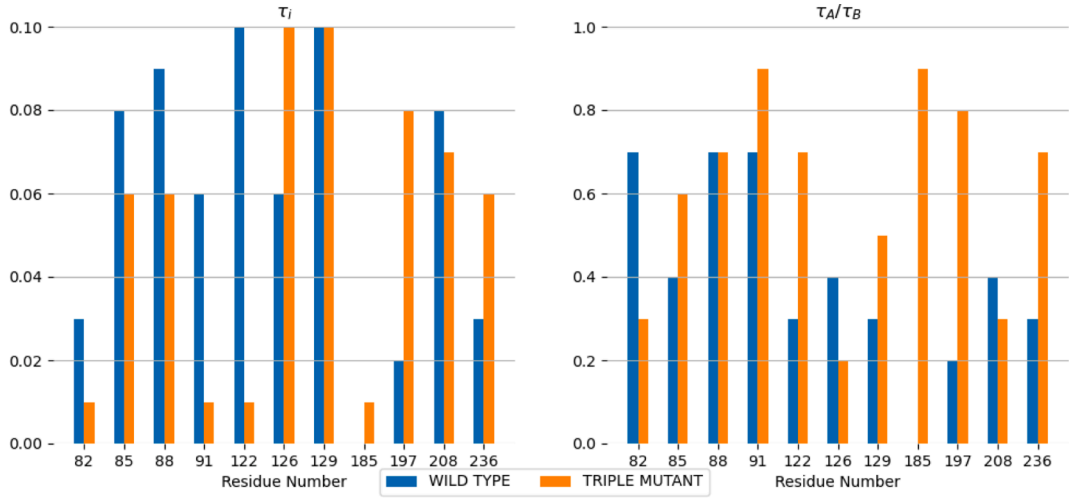

Fig. 7. Comparison of the obtained motional parameters between the proline residues of WT and TM OPN. The internal correlation times τ_i (in ns) and the values reporting the modulation of ring pucker (τ_A/τ_B) are reported on the left and right panels, respectively. The values for WT and TM are reported in blue and orange, respectively.

4. Conclusion

Summarizing, we presented a novel pulse scheme for measurement of dipole–dipole CCRs of $^{13}CH_2$ methylene groups in IDPs with exquisite spectral resolution. Constant-time evolution in the indirect carbon dimension not only gives narrow signals' lineshape but also allows for the quantification of CCR values. The pulse sequence is particularly suited to probe proline residues. The applicability of the experiment was illustrated with an application to OPN for which interesting changes in ring pucker dynamics were observed for a mutant form in which stabilizing interactions between proline and aromatic amino acid sidechains were disrupted.

We believe this to be particularly relevant for experimental studies of IDPs and their inherently local nature of spin relaxation. In contrast to their folded counterparts, spins in IDPs are not embedded within a fixed molecular tumbling frame. Extensive work using ^{15}N relaxation revealed interesting information on IDPs [46–50,60]. However, a single ^{15}N nucleus per residue as a dynamic probe is clearly not sufficient to adequately capture the underlying motions. In order to overcome this limitation, we have recently proposed a set of cross-correlated relaxation measurements probing chemical shift anisotropy (CSA) and dipole interference terms of backbone nuclei ^{15}N, $^{1}H^{N}$, $^{13}C'$ and $^{13}C^{\alpha}$ [60]. Properly detecting and quantifying the presence of anisotropy in IDP dynamics is an important prerequisite towards the molecular interpretation of NMR relaxation experiments. This is indispensable for the angular evaluation of cross-correlated relaxation (CCR) of remote spins and the determination of backbone dihedral angle distributions in IDPs [52].

Proline residues play a pivotal role in fundamental processes, e.g. protein–protein interactions, backbone rearrangements, post-translational modifications and secondary structure formation. We thus anticipate that the proposed pulse sequence might find numerous applications in IDP research and will support future NMR initiatives to characterize this eminent protein family in more detail.

Declaration of Competing Interest

The authors declare that they have no known competing financial interests or personal relationships that could have appeared to influence the work reported in this paper.

Data availability

Data will be made available on request.

Acknowledgement

The support of the CERM/CIRMMP center of Instruct-ERIC is gratefully acknowledged. This work was supported in part by the project "Potentiating the Italian Capacity for Structural Biology Services in Instruct-ERIC (ITACA.SB, Project no. IR0000009) within the call MUR 3264/2021 PNRR M4/C2/L3.1.1, funded by the European Union – Next Generation EU, by iNEXT-Discovery (PID 18874) funded by the Horizon 2020 program of the EC and by the Austrian Science Foundation (FWF, P 35098-B).

Appendix A. Supplementary material

Supplementary data to this article can be found online at https://doi.org/10.1016/j.jmr.2023.107539.

References

[1] P. Tompa, M. Fuxreiter, Fuzzy complexes: polymorphism and structural disorder in protein-protein interactions, Trends Biochem. Sci. 33 (2008) 2–8, https://doi.org/10.1016/j.tibs.2007.10.003.

[2] T. Mittag, L.E. Kay, J.D. Forman-Kay, Protein dynamics and conformational disorder in molecular recognition, J. Mol. Recognit. 23 (2009) 105–116, https://doi.org/10.1002/jmr.961.

[3] D. Kurzbach, T.C. Schwarz, G. Platzer, S. Höfler, D. Hinderberger, R. Konrat, Compensatory adaptations of structural dynamics in an intrinsically disordered protein complex, Angew, Chemie. 53 (2014) 3840–3843, https://doi.org/10.1002/anie.201308389.

[4] G.T. Heller, P. Sormanni, M. Vendruscolo, Targeting disordered proteins with small molecules using entropy, Trends Biochem. Sci. 40 (2015) 491–496, https://doi.org/10.1016/j.tibs.2015.07.004.

[5] G.T. Heller, F.A. Aprile, M. Vendruscolo, Methods of probing the interactions between small molecules and disordered proteins, Cell. Mol. Life Sci. 74 (2017) 3225–3243, https://doi.org/10.1007/s00018-017-2563-4.

[6] K. Tsafou, P.B. Tiwari, J.D. Forman-Kay, S.J. Metallo, J.A. Toretsky, Targeting intrinsically disordered transcription factors: changing the paradigm, J. Mol. Biol. 430 (2018) 2321–2341, https://doi.org/10.1016/j.jmb.2018.04.008.

[7] A. Sottini, A. Borgia, M.B. Borgia, K. Bugge, D. Nettels, A. Chowdhury, P. O. Heidarsson, F. Zosel, R.B. Best, B.B. Kragelund, B. Schuler, Polyelectrolyte interactions enable rapid association and dissociation in high-affinity disordered protein complexes, Nat. Commun. 11 (2020) 5736, https://doi.org/10.1038/s41467-020-18859-x.

[8] F. Parolini, R. Tira, C.G. Barracchia, F. Munari, S. Capaldi, M. D'Onofrio, M. Assfalg, Ubiquitination of Alzheimer's-related tau protein affects liquid-liquid phase separation in a site- and cofactor-dependent manner, Int. J. Biol. Macromol. 201 (2022) 173–181, https://doi.org/10.1016/j.ijbiomac.2021.12.191.

[9] P. Romero, Z. Obradovic, X. Li, E.C. Garner, C.J. Brown, A.K. Dunker, Sequence complexity of disordered protein, Proteins 42 (2001) 38–48, https://doi.org/10.1002/1097-0134(20010101)42:1<38::aid-prot50>3.0.co;2-3.

[10] J.A. Marsh, J.D. Forman-Kay, Sequence determinants of compaction in intrinsically disordered proteins, Biophys. J. 98 (2010) 2383–2390, https://doi.org/10.1016/j.bpj.2010.02.006.

[11] V.N. Uversky, J.R. Gillespie, A.L. Fink, Why are "natively unfolded" proteins unstructured under physiologic conditions? Proteins Struct. Funct. Genet. 41 (2000) 415–427, https://doi.org/10.1002/1097-0134(20001115)41:3<415::AID-PROT130>3.0.CO;2-7.

[12] A.K. Dunker, M.M. Babu, E. Barbar, M. Blackledge, S.E. Bondos, Z. Dosztányi, H. J. Dyson, J. Forman-Kay, M. Fuxreiter, J. Gsponer, K.-H. Han, D.T. Jones, S. Longhi, S.J. Metallo, K. Nishikawa, R. Nussinov, Z. Obradovic, R.V. Pappu, B. Rost, P. Selenko, V. Subramaniam, J.L. Sussman, P. Tompa, V.N. Uversky, What's in a name? Why these proteins are intrinsically disordered, Intrinsically Disord. Proteins. 1 (2013) e24157.

[13] F. Theillet, L. Kalmar, P. Tompa, K. Han, P. Selenko, A.K. Dunker, G.W. Daughdrill, V.N. Uversky, The alphabet of intrinsic disorder, Intrinsically Disord. Proteins. 1 (2013) e24360.

[14] J. Habchi, P. Tompa, S. Longhi, V.N. Uversky, Introducing protein intrinsic disorder, Chem. Rev. 114 (2014) 6561–6588, https://doi.org/10.1021/cr400514h.

[15] V.N. Uversky, Intrinsically disordered proteins and their "Mysterious" (Meta) Physics, Front. Phys. 7 (2019), https://doi.org/10.3389/fphy.2019.00010.

[16] B. Mateos, C. Conrad-Billroth, M. Schiavina, A. Beier, G. Kontaxis, R. Konrat, I. C. Felli, R. Pierattelli, The ambivalent role of proline residues in an intrinsically disordered protein: from disorder promoters to compaction facilitators, J. Mol. Biol. 432 (2020) 3093–3111, https://doi.org/10.1016/j.jmb.2019.11.015.

[17] J. Lopez, P. Ahuja, M. Gerard, J.-M. Wieruszeski, G. Lippens, A new strategy for sequential assignment of intrinsically unstructured proteins based on ^{15}N single isotope labelling, J. Magn. Reson. 236 (2013) 1–6, https://doi.org/10.1016/j.jmr.2013.07.007.

[18] Y. Yoshimura, N.V. Kulminskaya, F.A.A. Mulder, Easy and unambiguous sequential assignments of intrinsically disordered proteins by correlating the backbone ^{15}N or $^{13}C'$ chemical shifts of multiple contiguous residues in highly resolved 3D spectra, J. Biomol. NMR 61 (2015) 109–121, https://doi.org/10.1007/s10858-014-9890-7.

[19] S. Żerko, P. Byrski, P. Włodarczyk-Pruszyński, M. Górka, K. Ledolter, E. Masliah, R. Konrat, W. Koźmiński, Five and four dimensional experiments for robust backbone resonance assignment of large intrinsically disordered proteins: application to Tau3x protein, J. Biomol. NMR 65 (2016) 193–203, https://doi.org/10.1007/s10858-016-0048-7.

[20] I.C. Felli, R. Pierattelli, ^{13}C direct detected NMR for challenging systems, Chem. Rev. 122 (2022) 9468–9496, https://doi.org/10.1021/acs.chemrev.1c00871.

[21] A. Alik, C. Bouguechtouli, M. Julien, W. Bermel, R. Ghouil, S. Zinn-Justin, F. Theillet, Sensitivity-enhanced 13C-NMR spectroscopy for monitoring multisite phosphorylation at physiological temperature and pH, Angew. Chemie Int. Ed. 59 (2020) 10411–10415, https://doi.org/10.1002/anie.202002288.

[22] F.-X. Theillet, C. Smet-Nocca, S. Liokatis, R. Thongwichian, J. Kosten, M.-K. Yoon, R.W. Kriwacki, I. Landrieu, G. Lippens, P. Selenko, Cell signaling, post-translational protein modifications and NMR spectroscopy, J. Biomol. NMR 54 (2012) 217–236, https://doi.org/10.1007/s10858-012-9674-x.

[23] K. Takeuchi, G. Heffron, Z.Y.J. Sun, D.P. Frueh, G. Wagner, Nitrogen-detected CAN and CON experiments as alternative experiments for main chain NMR resonance assignments, J. Biomol. NMR 47 (2010) 271–282, https://doi.org/10.1007/s10858-010-9430-z.

[24] S. Mäntylahti, M. Hellman, P. Permi, Extension of the HA-detection based approach: (HCA)CON(CA)H and (HCA)NCO(CA)H experiments for the main-chain assignment of intrinsically disordered proteins, J. Biomol. NMR 49 (2011) 99–109, https://doi.org/10.1007/s10858-011-9470-z.

[25] H. Kovacs, D. Moskau, M. Spraul, Cryogenically cooled probes - A leap in NMR technology, Prog. Nucl. Magn. Reson. Spectrosc. 46 (2005) 131–155, https://doi.org/10.1016/j.pnmrs.2005.03.001.

[26] W. Bermel, I. Bertini, I.C. Felli, R. Kümmerle, R. Pierattelli, Novel ^{13}C direct detection experiments, including extension to the third dimension, to perform the complete assignment of proteins, J. Magn. Reson. 178 (2006) 56–64, https://doi.org/10.1016/j.jmr.2005.08.011.

[27] D. Sahu, M. Bastidas, S.A. Showalter, Generating NMR chemical shift assignments of intrinsically disordered proteins using carbon-detected NMR methods, Anal. Biochem. 449 (2014) 17–25, https://doi.org/10.1016/j.ab.2013.12.005.

[28] E.C. Cook, G.A. Usher, S.A. Showalter, The use of ^{13}C direct-detect NMR to characterize flexible and disordered proteins, Methods Enzymol. 611 (2018) 81–100, https://doi.org/10.1016/bs.mie.2018.08.025.

[29] E.B. Gibbs, R.W. Kriwacki, Direct detection of carbon and nitrogen nuclei for high-resolution analysis of intrinsically disordered proteins using NMR spectroscopy, Methods 2 (2018) 2–9, https://doi.org/10.1016/j.ymeth.2018.01.004.

[30] W. Bermel, M. Bruix, I.C. Felli, M.V. Kumar, R. Pierattelli, S. Serrano, Improving the chemical shift dispersion of multidimensional NMR spectra of intrinsically disordered proteins, J. Biomol. NMR 55 (2013) 231–237, https://doi.org/10.1007/s10858-013-9704-3.

[31] W. Bermel, I. Bertini, I.C. Felli, Y.M. Lee, C. Luchinat, R. Pierattelli, Protonless NMR experiments for sequence-specific assignment of backbone nuclei in unfolded proteins, J. Am. Chem. Soc. 128 (2006) 3918–3919, https://doi.org/10.1021/ja0582206.

[32] M.G. Murrali, A. Piai, W. Bermel, I.C. Felli, R. Pierattelli, Proline fingerprint in intrinsically disordered proteins, Chembiochem 19 (2018) 1625–1629, https://doi.org/10.1002/cbic.201800172.

[33] M. Schiavina, M.G. Murrali, L. Pontoriero, V. Sainati, R. Kümmerle, W. Bermel, R. Pierattelli, I.C. Felli, Taking simultaneous snapshots of intrinsically disordered proteins in action, Biophys. J. 117 (2019) 46–55, https://doi.org/10.1016/j.bpj.2019.05.017.

[34] A. Piai, E.O. Calcada, T. Tarenzi, A. Grande, M. Varadi, P. Tompa, I.C. Felli, R. Pierattelli, Article just a flexible linker ? The structural and dynamic properties of CBP-ID4 revealed by NMR spectroscopy, Biophys. J. 110 (2016) 372–381, https://doi.org/10.1016/j.bpj.2015.11.3516.

[35] K. Kloiber, R. Konrat, Peptide plane torsion angles in proteins through intraresidue 1H–^{15}N–^{13}C‘ Dipole−CSA relaxation interference: facile discrimination between Type-I and Type-II β-turns, J. Am. Chem. Soc. 122 (2000) 12033–12034, https://doi.org/10.1021/ja002314s.

[36] H. Schwalbe, T. Carlomagno, M. Hennig, J. Junker, B. Reif, C. Richter, C. Griesinger, Cross-correlated relaxation for measurement of angles between tensorial interactions, Methods Enzymol. 338 (2001) 35–81, https://doi.org/10.1016/s0076-6879(02)38215-6.

[37] L. Emsley, G. Bodenhausen, Gaussian pulse cascades: New analytical functions for rectangular selective inversion and in-phase excitation in NMR, Chem. Phys. Lett. 165 (1990) 469–476, https://doi.org/10.1016/0009-2614(90)87025-M.

[38] W. Bermel, I. Bertini, L. Duma, I.C. Felli, L. Emsley, R. Pierattelli, P.R. Vasos, Complete assignment of heteronuclear protein resonances by protonless NMR spectroscopy, Angew. Chemie Int. Ed. 44 (2005) 3089–3092, https://doi.org/10.1002/anie.200461794.

[39] W. Bermel, I. Bertini, V. Csizmok, I.C. Felli, R. Pierattelli, P. Tompa, H-start for exclusively heteronuclear NMR spectroscopy: The case of intrinsically disordered proteins, J. Magn. Reson. 198 (2009) 275–281, https://doi.org/10.1016/j.jmr.2009.02.012.

[40] D. Yang, A. Mittermaier, Y.-K. Mok, L.E. Kay, A study of protein side-chain dynamics from new ^{2}H auto-correlation and ^{13}C cross-correlation NMR experiments: application to the N-terminal SH3 domain from drk1, J. Mol. Biol. 276 (1998) 939–954, https://doi.org/10.1006/jmbi.1997.1588.

[41] Y. Zheng, D. Yang, Measurement of dipolar cross-correlation in methylene groups in uniformly ^{13}C,^{15} N-labeled proteins, J. Biomol. NMR 28 (2004) 103–116, https://doi.org/10.1023/B:JNMR.0000013826.82936.0e.

[42] L. Banci, I. Bertini, I.C. Felli, P. Hajieva, M.S. Viezzoli, Side chain mobility as monitored by CH-CH cross correlation: The example of cytochrome b_5, J. Biomol. NMR 20 (2001) 1–10, https://doi.org/10.1023/A:1011245101351.

[43] W. Bermel, I. Bertini, J. Chill, I.C. Felli, N. Haba, M.V. Kumar, R. Pierattelli, Exclusively heteronuclear ^{13}C-detected amino-acid-selective NMR experiments for the study of intrinsically disordered proteins (IDPs), Chembiochem 13 (2012) 2425–2432, https://doi.org/10.1002/cbic.201200447.

[44] V. Ozenne, F. Bauer, L. Salmon, J.R. Huang, M.R. Jensen, S. Segard, P. Bernadó, C. Charavay, M. Blackledge, Flexible-meccano: A tool for the generation of explicit ensemble descriptions of intrinsically disordered proteins and their associated experimental observables, Bioinformatics 28 (2012) 1463–1470, https://doi.org/10.1093/bioinformatics/bts172.

[45] M. Kadkhodaie, O. Rivas, M. Tan, A. Mohebbi, A. Shaka, Broadband homonuclear cross polarization using flip-flop spectroscopy, J. Magn. Reson. 91 (1991) 437–443, https://doi.org/10.1016/0022-2364(91)90210-K.

[46] T. Yuwen, N.R. Skrynnikov, Proton-decoupled CPMG: A better experiment for measuring ^{15}N R_2 relaxation in disordered proteins, J. Magn. Reson. 241 (2014) 155–169, https://doi.org/10.1016/j.jmr.2013.08.008.

[47] M.L. Gill, R.A. Byrd, A.G. Palmer III, Dynamics of GCN4 facilitate DNA interaction: a model-free analysis of an intrinsically disordered region, PCCP 18 (2016) 5839–5849, https://doi.org/10.1039/C5CP06197K.

[48] C. Charlier, S.F. Cousin, F. Ferrage, Protein dynamics from nuclear magnetic relaxation, Chem. Soc. Rev. 45 (2016) 2410–2422, https://doi.org/10.1039/C5CS00832H.

[49] N. Salvi, A. Abyzov, M. Blackledge, Atomic resolution conformational dynamics of intrinsically disordered proteins from NMR spin relaxation, Prog. Nucl. Magn. Reson. Spectrosc. 102–103 (2017) 43–60, https://doi.org/10.1016/j.pnmrs.2017.06.001.

[50] S. Chhabra, P. Fischer, K. Takeuchi, A. Dubey, J.J. Ziarek, A. Boeszoermenyi, D. Mathieu, W. Bermel, N.E. Davey, G. Wagner, H. Arthanari, ^{15}N detection harnesses the slow relaxation property of nitrogen: Delivering enhanced resolution for intrinsically disordered proteins, Proc. Natl. Acad. Sci. (2018) 201717560, https://doi.org/10.1073/pnas.1717560115.

[51] V.A. Daragan, K.H. Mayo, Motional model analyses of protein and peptide dynamics using ^{13}C and ^{15}N NMR relaxation, Prog. Nucl. Magn. Reson. Spectrosc. 31 (1997) 63–105, https://doi.org/10.1016/S0079-6565(97)00006-X.

[52] N. Salvi, A. Abyzov, M. Blackledge, Solvent-dependent segmental dynamics in intrinsically disordered proteins, Sci. Adv. 5 (2019), https://doi.org/10.1126/sciadv.aax2348.

[53] D. Das, S. Mukhopadhyay, Molecular origin of internal friction in intrinsically disordered proteins, Acc. Chem. Res. 55 (2022) 3470–3480, https://doi.org/10.1021/acs.accounts.2c00528.

[54] A. Abyzov, E. Mandelkow, M. Zweckstetter, N. Rezaei-Ghaleh, Fast motions dominate dynamics of intrinsically disordered tau protein at high temperatures, Chem. – A Eur. J. 29 (2023), https://doi.org/10.1002/chem.202203493.

[55] G. Lipari, A. Szabo, Model-free approach to the interpretation of nuclear magnetic resonance relaxation in macromolecules. 2. Analysis of experimental results, J. Am. Chem. Soc. 104 (1982) 4559–4570, https://doi.org/10.1021/ja00381a010.

[56] R.E. London, The interpretation of carbon-13 spin-lattice relaxation resulting from ring puckering in proline, J. Am. Chem. Soc. 100 (1978) 2678–2685, https://doi.org/10.1021/ja00477a018.

[57] S.C. Shekar, K.R.K. Easwaran, Proline ring conformations corresponding to a bistable jump model from13C spin-lattice relaxation times, Biopolymers 21 (1982) 1479–1487, https://doi.org/10.1002/bip.360210802.

[58] D. Mikhailov, V.A. Daragan, K.H. Mayo, ^{13}C multiplet nuclear magnetic resonance relaxation-derived ring puckering and backbone dynamics in proline-containing glycine-based peptides, Biophys. J. 68 (1995) 1540–1550, https://doi.org/10.1016/S0006-3495(95)80326-7.

[59] D. Mikhailov, V. Daragan, K. Mayo, Lysine side-chain dynamics derived from ^{13}C-multiplet NMR relaxation studies on di- and tripeptides, J. Biomol. NMR 5 (1995), https://doi.org/10.1007/BF00182283.

[60] C. Kauffmann, I. Ceccolini, G. Kontaxis, R. Konrat, Detecting anisotropic segmental dynamics in disordered proteins by cross-correlated spin relaxation, Magn. Reson. 2 (2021) 557–569, https://doi.org/10.5194/mr-2-557-2021.